A hybrid framework for single tree detection from airborne laser scanning data: A case study in temperate mature coniferous forests in Ontario, Canada

CrossMark

Junjie Zhang [a,1], Gunho Sohn [a,*], Mathieu Brédif [b,2]

[a] GeoICT Lab, Department of Earth and Space Science & Engineering, York University, 4700 Keele Street, Toronto, ON M3J 1P3, Canada
[b] Université Paris Est, IGN, MATIS 73, avenue de Paris, 94165 Saint-Mandé, France

A B S T R A C T

This study presents a hybrid framework for single tree detection from airborne laser scanning (ALS) data by integrating low-level image processing techniques into a high-level probabilistic framework. The proposed approach modeled tree crowns in a forest plot as a configuration of circular objects. We took advantage of low-level image processing techniques to generate candidate configurations from the canopy height model (CHM): the treetop positions were sampled within the over-extracted local maxima via local maxima filtering, and the crown sizes were derived from marker-controlled watershed segmentation using corresponding treetops as markers. The configuration containing the best possible set of detected tree objects was estimated by a global optimization solver. To achieve this, we introduced a Gibbs energy, which contains a data term that judges the fitness of the objects with respect to the data, and a prior term that prevents severe overlapping between tree crowns on the configuration space. The energy was then embedded into a Markov Chain Monte Carlo (MCMC) dynamics coupled with a simulated annealing to find its global minimum. In this research, we also proposed a Monte Carlo-based sampling method for parameter estimation. We tested the method on a temperate mature coniferous forest in Ontario, Canada and also on simulated coniferous forest plots with different degrees of crown overlap. The experimental results showed the effectiveness of our proposed method, which was capable of reducing the commission errors produced by local maxima filtering, thus increasing the overall detection accuracy by approximately 10% on all of the datasets.

© 2014 International Society for Photogrammetry and Remote Sensing, Inc. (ISPRS). Published by Elsevier B.V. All rights reserved.

1. Introduction

1.1. Airborne laser scanning in forest inventory

Remote sensing techniques have become an integral part of forest inventory to provide accurate, precise and timely forest and tree characteristics at different scales to support practices of forest management and planning (Dubayah and Drake, 2000; Naesset et al., 2004; Tomppo et al., 2002; Wulder, 1998; Xie et al., 2008). Among these techniques, small-footprint airborne laser scanning (ALS), also known as airborne LiDAR, has rapidly gained popularity in forest inventory in recent decades. The unique capability of ALS to directly measure the 3D structural information of trees and the

elevation of the terrestrial surface under the canopy in forests makes ALS an alternative to traditional passive optical remote sensing technology, or even the preferred method, to derive certain forest parameters, such as canopy height, crown dimensions, stand volume, basal area, and above-ground biomass (Bortolot and Wynne, 2005; Hyyppä and Inkinen, 1999; Means et al., 2000; Næsset, 1997; Naesset, 2002).

Characterization of forest resources using ALS can be broadly categorized into area-based approaches (ABAs) and individual-tree-based approaches (ITDs) (Hyyppä et al., 2008). ABAs rely on the statistical principle and predicts forest attributes based on parametric regression or nonparametric imputation models built between field measured variables and features derived from ALS data (Maltamo et al., 2006; Naesset, 2002). ABAs can perform under a low ALS point density, and is the method currently applied in operational forest inventory to provide a wall-to-wall estimation of forest attributes (Naesset, 2004; White et al., 2013). ITDs measure or predict tree-level variables on the basic unit of the

individual trees from ALS data and then aggregate them to obtain stand-level forest inventory results (Hyyppä et al., 2012).

Despite the added costs and amount of information to store and process high-density ALS data, ITDs are of significant interest in forest inventory and is a motivating research topic. The primary advantage of ITDs over ABAs is the supply of tree lists and the ability to directly derive the true stem distribution series, which would result in better prediction for timber assortments (Vastaranta et al., 2011a). Generally, this information is invaluable in forest planning-related simulation and optimization, logging operation planning and wood supply logistics (Vastaranta et al., 2011b), e.g., detection of harvest trees and forest growth determination (Yu et al., 2004). Another advantage of ITDs is that they can reduce the amount of or potentially replace the expensive fieldwork required for ABAs (Hyyppä et al., 2008; Vastaranta et al., 2012). Additionally, tree species classification based on ITD has been reported in recent studies (Brandtberg, 2007; Heinzel and Koch, 2011; Orka et al., 2009; Suratno et al., 2009), which could potentially improve the prediction of species-specific forest attributes (Heurich, 2008; Yao et al., 2012; Yu et al., 2010). Furthermore, the combination of ITD and ABA, called the semi-ITD method, to improve the estimation accuracy has also been viewed as a future method for forest inventory (Breidenbach et al., 2010; Hyyppä et al., 2012; Vastaranta et al., 2012). Therefore, individual tree detection techniques are still of significant importance from the practical forestry viewpoint.

1.2. Related works on single tree detection

Accordingly, numerous methods have been proposed to detect single trees from ALS data. Most of the methods focus on the generation of the canopy height model (CHM), which provides an accurate representation of the outer surface of the tree canopy. The peaks and valleys on the CHM generated from high-density ALS data are better estimations of treetop positions and crown edges than can be obtained from aerial photographs or satellite imageries. Therefore, many studies have extended methods developed for passive optical imageries to detect single trees from ALS data. Those methods include, but are not limited to, local maxima filtering (Popescu et al., 2002; Wulder et al., 2000), region growing (Erikson, 2003; Solberg et al., 2006), valley following (Gougeon, 1995; Leckie et al., 2003), template matching (Korpela et al., 2007; Pollock, 1996), watershed segmentation and its variance marker-controlled watershed segmentation (Chen et al., 2006; Pyysalo and Hyyppa, 2002; Wang et al., 2004), and multi-scale segmentation (Brandtberg and Walter, 1998; Brandtberg et al., 2003).

Among the proposed methods, local maxima filtering (LM) and marker-controlled watershed segmentation (MCWS) are the most commonly used and are ready for operational application because of their rapid implementation while maintaining the capability to produce relatively accurate results (Kaartinen et al., 2012). Popescu et al. (2002) have been the first to test a variable window local maxima filtering on the CHMs, attempting to overcome errors of omission and commission associated with fixed window local maxima filtering (Hyyppä et al., 2001).

Once the treetops are detected, MCWS is well suited to delineate the tree crown segments from the CHM. MCWS, which possesses the advantages of other segmentation methods of region growing and edge detection, was introduced by Meyer and Beucher (1990) to overcome the over-segmentation problem of ordinary watershed segmentation. In MCWS, user-specified markers are used as the marker function to perform the segmentation; for additional details, see Gonzalez and Woods (2008). In the resultant segmentation, there will be one segment corresponding to each marker; in the case of single tree detection, one tree crown will be captured by one treetop. This result indicates the detection

accuracy of MCWS, subject to the accuracy of the pre-determined local maxima as true treetops in the previous stage.

The issue with LM is the selection of the filter window size and the determination of the relationship between the crown size and the tree height. In the comparison of tree detection algorithms (Kaartinen et al., 2012), the local maxima-based approach tends to produce high commission errors. Especially in coniferous forests, spurious treetops are detected within the tree crowns from large branches. In other cases, local maxima filtering produces a low commission error, and the omission error often increases because small tree crowns are more likely to be undetected (Gebreslasie et al., 2011).

1.3. Probabilistic methods for image analysis

Probabilistic methods represent another branch of powerful tools in image analysis. These methods have proven to hold great promise in solving inverse problems, including image segmentation, image restoration, and feature extraction (Descombes and Zerubia, 2002). In particular, stochastic models have evolved from random fields to object processes, and the work has shifted from an early focus on 'low-level' tasks that aim to de-noise, sharpen, and segment images to solving 'high-level' tasks of feature recognition, i.e., describing an image by its content (Van Lieshout, 2009). Additional details on low-level and high-level image analysis tasks can be found in Sonka et al. (2008).

Marked point processes, detailed in Van Lieshout (2000), are among the most efficient stochastic models used to exploit the random variables whose realizations are configurations of geometric objects or shapes. Generally, in these processes, after a probability distribution measuring the quality of each object configuration is defined in the configuration space, the maxima density estimator is searched for by the Markov Chain Monte Carlo (MCMC) sampler (Hastings, 1970) coupled with conventional simulated annealing (Metropolis et al., 1953). This process has led to convincing experimental results in various image analysis and feature extraction applications, such as road networks extraction (Lacoste et al., 2005), road mark detection (Tournaire and Paparoditis, 2009), and 3D building reconstruction (Lafarge et al., 2008; Ortner et al., 2008; Tournaire et al., 2010).

Likewise, several stochastic models have been proposed to detect tree crowns from remote sensing data. Descombes and Pechersky (2006) have presented a three-state Markov Random Field (MRF) model to detect the tree crowns from aerial imageries. This approach addressed the problem as an image segmentation problem and works on the pixel level. Each pixel is assigned to one of the following three states: (i) *vegetation*, (ii) *background,* and (iii) *center of trees*. Although the MRF was defined on the pixel level, the label update was performed on the object level using elliptical templates of crowns. Furthermore, Perrin et al. (2005, 2006) has employed marked point processes to detect tree crowns in plantations from color infrared (CIR) aerial imageries. Tree crowns in the remote sensing image are modeled as a configuration of disks or ellipses. In both of the studies, tree crowns were detected by maximizing a Bayesian criterion, such as *Maximum A Posteriori* (MAP), which became an energy minimization problem and was solved in a simulated annealing framework.

These stochastic models provide a powerful framework to allow the inclusion of spatial interactions between objects in the prior while enabling a measure of consistency between objects and the image in the data term. However, the inherited property of stochastic models requires exploration of a large configuration space searching for the optimal configuration, especially for non-data-driven models, which do not employ any low-level information that can be extracted from the images. The optimization process is typically lengthy and computationally expensive.

1.4. Proposed framework and organization of the paper

This study presents a hybrid framework used to detect single trees from ALS data by integrating the low-level image processing techniques, i.e., LM and MCWS, into a high-level probabilistic model. The proposed model aims to improve the detection accuracy compared with traditional LM. Moreover, this model samples in a reduced configuration space by utilizing image features extracted by LM and MCWS, which potentially accelerate the optimization process compared with classical stochastic models, e.g., marked point processes. The estimation of parameters is another issue. In most cases, the parameters are tuned by trial and error. We address the problem of parameter estimation by proposing a Monte Carlo based method.

This paper is organized as follows. Section 2 describes the study area and the data used in the study. Section 3 is dedicated to the formulation of our proposed model. We provide an overview of the general framework of energy modeling for the stochastic model, followed by detailing the model design from the configuration space definition to the energy formulation, parameter estimation and model optimization. Finally, an accuracy assessment method is included. The experimental results of the parameter estimation and tree detection on real and simulated ALS data are given in Section 4, and Section 5 presents a discussion on the proposed model and the achieved results. Conclusions and certain perspectives for future studies are outlined in Section 6.

2. Materials

2.1. Study area

The study area is a temperate mature coniferous forest located in the Great Lakes-St. Lawrence region approximately 60 km east of Sault Ste. Marie, Ontario, Canada (Fig. 1(a)). The natural vegetation dominant in the coniferous forest is eastern white pine (*Pinus strobus*) and jack pine (*Pinus banksiana*), mixed with some red pine (*Pinus resinosa*) and black spruce (*Picea mariana*). The forest has an intermediate dense canopy with some open space. The canopy height is homogenous with an average height of approximately 20 m. There are some small white pines and shrubs growing in the understory with a height of approximately 2–3 m (Fig. 1(b) and (c)).

2.2. Field survey

To test the proposed single tree detection model, three plots with sizes of 82 × 95 m, 50 × 50 m and 80 × 80 m were selected, and a field survey was conducted in August 2009. The forest mensuration campaign determined the tree height (h_i, m) with a Vertex hypsometer and the diameter at beast height (DBH) with a DBH tape. The positions of trees with a height greater than 5 m ($h_i \geqslant 5$) were determined using GPS and the total station. The crown width and species were also measured and recorded. The stem densities of trees with a value of $h_i \geqslant 5$ are 154/ha, 160/ha and 190/ha, with increasing values for the three study plots.

2.3. Airborne laser scanning data

The ALS data were acquired over the study area by a Riegl LMS-Q560 laser scanner during the same period as the field work. The flight was performed at a height of approximately 300 m above the ground with a maximum scanning angle of 22.5°, rendering a swath width of approximately 300 m. The flight line was designed to pass over the planned forest plots; therefore, they were located in the middle part of the swath, and the obscure effect of the crowns can be minimized for the plots of interest. The device recorded full-waveforms that were processed into discrete point clouds with up to 5 returns per pulse. The data collection configuration yielded a high point density of approximately 30 points per
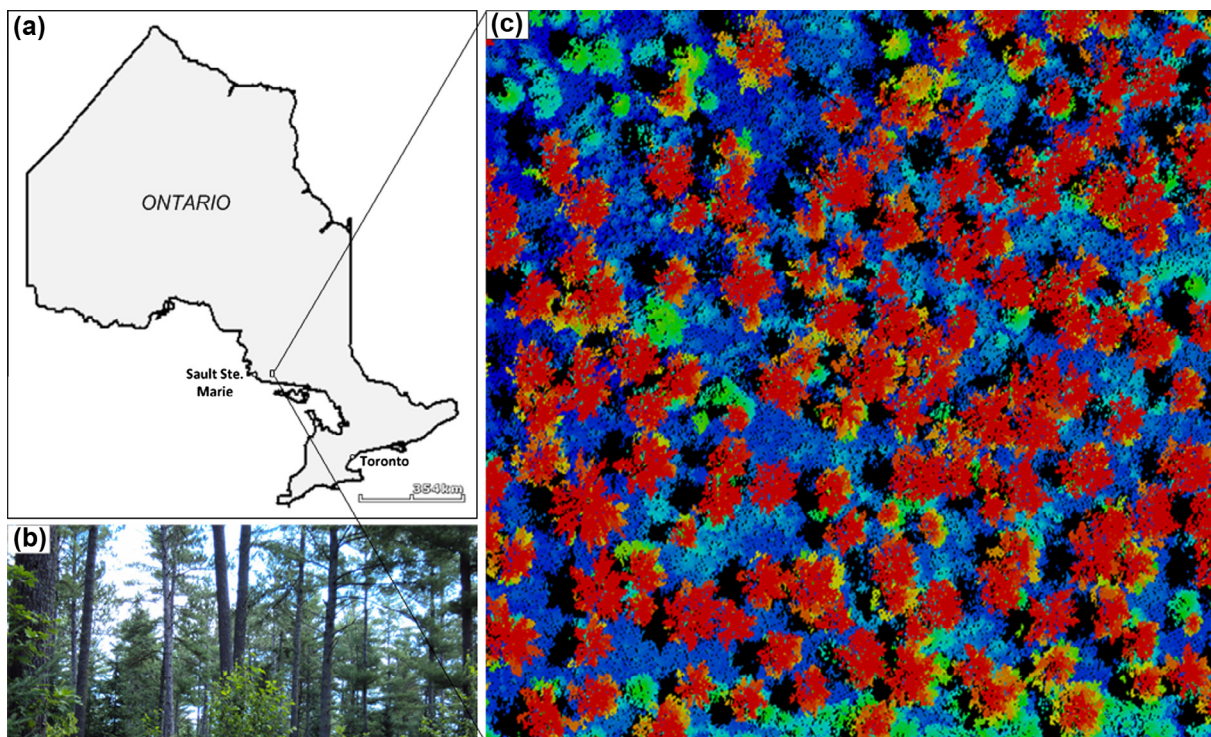

Fig. 1. (a) Location of the study area in the Province of Ontario, Canada; (b) a photo and (c) ortho view of the ALS data of a forest plot in the study area rendered by height.

m^2 over the forested area. The returns were classified as ground and vegetation points using TerraScan software (TerraSolid Ltd., Helsinki, Finland). The CHM with a resolution of 0.5 m was derived as the difference between the digital surface model (DSM) and the digital elevation model (DEM), interpolated from vegetation points and ground points, respectively (Hyyppä et al., 2001).

2.4. Simulated ALS data

Vauhkonen et al. (2012) noted that the performance of the ITD algorithms typically depends on the tree density and the spatial distribution of trees, i.e., clustering patterns. To test the robustness of the proposed model more thoroughly, simulated ALS data of coniferous forest plots with a higher stem density than real forest plots and different degrees of crown overlap were also prepared in our study. First, three forest plots, each with a size of 100 × 100 m, were generated with a hard-core process in which the crown overlap was controlled by the interaction distance specified in the hard-core process. The smaller the interaction distance in the hard-core process, the more likely the tree objects will be overlapped in the resultant plots. Fig. 2(a)–(c) shows the three resulting point processes. With an increasing degree of crown overlap, the tree density in the plots also increases. The stem densities of trees with a value of $h_i \geqslant 5$ in the three forest plots are 186/ha, 234/ha and 261/ha, respectively.

ALS point clouds of individual trees were then selected according to the crown size from a coniferous tree template library and placed in each position to synthesize the ALS data of the forest plot. The tree template library was prepared from ALS data acquired from the study area we surveyed. A more detailed procedure can be found in Zhang and Sohn (2010). The generated ALS point clouds viewed from the nadir direction are shown in Fig. 2(d)–(f). The plots from left to right show forest plots with separated, touching and overlapping tree crowns, respectively.

In the simulated forest plots, the tree position, height and crown size are exactly known, therefore providing ideal reference data to examine the performance of our proposed model under different forest conditions. The simulated ALS data can also be used to validate the parameter estimation method proposed in Section 3.5 and to investigate the influence that the degree of crown overlap has on the parameter setting in the proposed model.

3. Methodology

3.1. General framework of energy modeling for the stochastic models

In a probabilistic framework, feature extraction or object detection from remotely sensed data can be viewed as an inverse problem. In object oriented stochastic models, features or objects are represented as a configuration of geometric shapes or objects. To find the best configuration **x** based on the observed data **y** (the image), we must find the configuration $\hat{\mathbf{x}}$ maximizing the posterior probability, according to the following equation:

$$\hat{\mathbf{x}} = \underset{\mathbf{x}\in\Omega}{\mathrm{argmax}}\, \mathbb{P}(X = \mathbf{x}|Y = \mathbf{y}) \tag{1}$$

where Ω is the configuration space in which **x** resides. X and Y are two random variables.

The probability of the model can also be specified in the form of a Gibbs energy $U(\mathbf{x})$, which implicitly depends on the constant value **y** given by the observation:
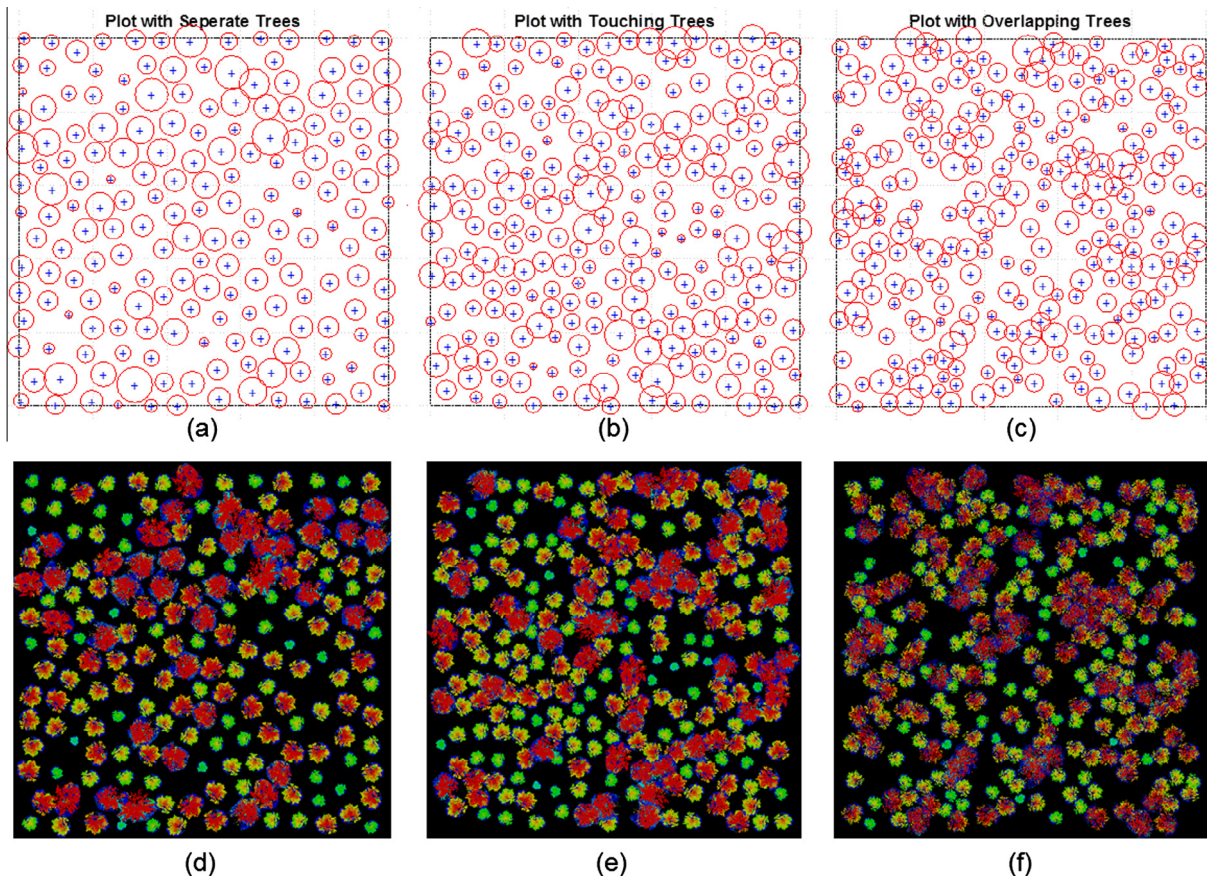

Fig. 2. (a)–(c) Point process simulated forest plots with different degrees of crown overlap: (a) plot with separated crowns; (b) plot with tree crowns slightly touching each other; (c) plot with overlapping crowns. (d)–(f) The corresponding ALS point clouds of the three forest plots generated.

$$\mathbb{P}(X = \mathbf{x}|Y = \mathbf{y}) = \frac{1}{Z}e^{-U(\mathbf{x})} \qquad (2)$$

where Z is a normalizing constant such that $Z = \int_{\mathbf{x} \in \Omega} e^{-U(\mathbf{x})}$. The issue is then reduced to the energy minimization problem of finding the *Maximum A Posteriori* estimator $\hat{\mathbf{x}} = \text{argmax}_{\mathbf{x} \in \Omega} \mathbb{P}(X = \mathbf{x}|Y = \mathbf{y})$, which is equivalent to finding the configuration minimizing the Gibbs energy $U(\cdot)$, i.e., $\hat{\mathbf{x}} = \text{argmin}_{\mathbf{x} \in \Omega} U(\mathbf{x})$. Generally, an MCMC embedded simulated annealing is used to find the optimal configuration $\hat{\mathbf{x}}$. The optimization process is particularly interesting because the complex computation of the normalizing constant Z is avoided.

3.2. Overall workflow of the proposed model

The flow chart of the proposed method is shown in Fig. 3. As our primary contribution, the blue blocks show the process how we construct a constrained configuration space for tree detection, by taking advantages of low-level image processing techniques, which is detailed in Section 3.3. The red block involves techniques of energy formulation and parameter estimation, which are covered in Sections 3.4 and 3.5, respectively. The optimization process illustrated by the yellow blocks is described in Section 3.6.

3.3. Configuration space definition of the proposed model

Let us first recall the configuration space definition in the marked point process. In remote sensing images, the distribution of tree crowns in forests can be represented by a marked point process of disks. The associated space $\mathcal{S}$ can be written according to the following equation:

$$\mathcal{S} = \mathcal{P} \times \mathcal{M} = [0, X_M] \times [0, Y_M] \times [r_m, r_M] \qquad (3)$$

where X_M and Y_M are the width and height of the image $\mathcal{J}$, respectively, and (r_m, r_M) are the minimum and maximum radii of the disks in the configuration, respectively. Note that $x = (p, r) \in \mathcal{S}$ is a tree object, where $p \in \mathcal{P}$ is its position and $r \in \mathcal{M}$ its radius. The configuration space Ω of the marked point process of the tree crowns can be written according to the following equation:

$$\Omega = \bigcup_{n=0}^{\infty} \Omega_n, \Omega_n = \{\{x_1, \ldots, x_n\} \subset \mathcal{S}\} \qquad (4)$$

that contains all of the configurations of a finite number of tree objects x_i of $\mathcal{S}$.

In this study, we seek to construct a constrained configuration space $\Omega_T \subset \Omega$ in which the optimal or near optimal configuration resides. We will then limit the search for the optimal configuration in the constrained space Ω_T, which could significantly reduce the computation demand of random sampling in Ω in the optimization process.

We begin by constructing a CHM image, representing the height of the tree crowns above ground from the classified ALS data. Then, we extract the local maxima as potential treetops from the CHM using local maxima filtering with a variable window size method adapted from Popescu et al. (2002). Our rule is to detect as many true treetops and reduce omission errors in the first stage. Therefore, the filters of the LM are set with relative small size empirically based on the *priori* knowledge about the plots to over-populate initial 'treetops'. Let T represents the set of extracted local maxima: $T = \{t_1, \ldots, t_N\}, \forall i \in \{1, \ldots, N\}, t_i \in \mathcal{P}$, where N is the total number of local maxima extracted. The true treetops within the set of local maxima T are noted as $T^{\circ} \subset T$.

Given any subset of local maxima $C \subset T$, they can be used as markers in marker-controlled watershed segmentation to obtain a partition $S(C) = \{S_{C_1}, \ldots, S_{C_{n(C)}}\}$ of the CHM, where S_{C_i} is the corresponding segment of the local maxima $t_{C_i} \in C$. $S(C)$ is a low-level presentation of the CHM image, and the set of segments are assumed to be a reasonable approximation of the tree crowns with respect to the set of local maxima C, where $n(C)$ is the number of local maxima in C.

A tree object $x_{C_i} = (t_{C_i}, r_{C_i})$ is then defined by its location and radius on the segment S_{C_i}, where the tree location is the corresponding local maximum t_{C_i}, and the radius r_{C_i} is calculated as the average radius of the segment S_{C_i}. A configuration $\mathbf{x}(C) = \{x_{C_1}, \ldots, x_{C_{n(C)}}\}$ is then constructed from the set of local maxima C. The entire procedure of configuration construction is illustrated in Fig. 4.

We note all of the configurations generated from the subsets of local maxima T as $\Omega_T = \{\mathbf{x}(C), C \subset T\}$. Apparently, Ω_T is a discrete subspace of the configuration space Ω, which cardinality is $\text{card}(\{\mathbf{x}(C), C \subset T\}) = \text{card}(\{C, C \subset T\}) = 2^{\text{card}(T)}$. In this manner, we build a constrained configuration space Ω_T from which to sample the optimal configuration.

3.4. Energy formulation

As previously mentioned, the Gibbs energy $U(\mathbf{x})$ is defined on the configuration space to measure the goodness or cost of each object configuration. The Gibbs energy can be further expressed as a weighted sum of a prior term $U_p(\mathbf{x})$ that favors a specific spatial pattern in configuration $\mathbf{x}$ and a data term $U_d(\mathbf{x})$ that quantifies the quality of the configuration with respect to the data, according to the following equation:

$$U(\mathbf{x}) = \alpha U_d(\mathbf{x}) + (1 - \alpha)U_p(\mathbf{x}) \qquad (5)$$

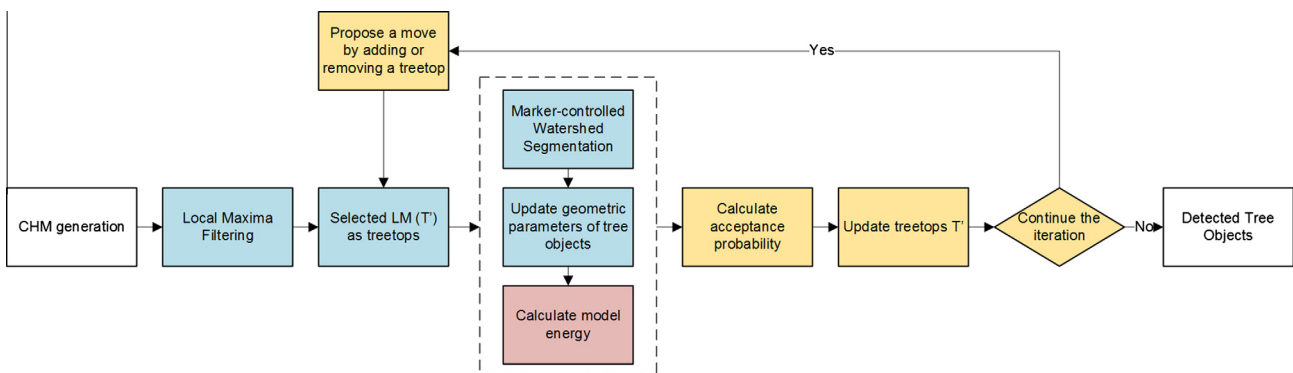where $\alpha \in [0, 1]$ specifies the relative weights of the two energy terms.

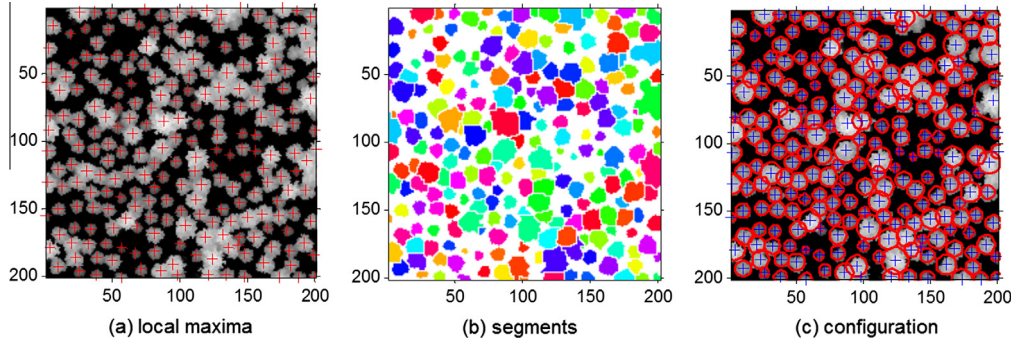**Fig. 3.** Flow chart of the proposed method.

Fig. 4. An example showing the configuration construction from a CHM. (a) A subset of local maxima. Local maxima are shown as red crosses; (b) a marked-controlled watershed segmentation of the CHM using local maxima in (a) as the marker function; (c) the configuration constructed from the local maxima. Radii of the tree crowns are extracted from the corresponding segments in (b).

We intend to make simple and effective choices for the design of each energy term. The basic assumptions are the geometric properties of trees in mature coniferous forests in which treetops are typically located in the central part of tree crowns, and tree crowns are of a circular shape when viewed from the nadir direction (Chen et al., 2006; Gleason and Im, 2012). We also tend to penalize certain patterns in the configurations in the prior term that tree crowns should not severely overlap.

3.4.1. Data term

The data term is in accordance with the aforementioned assumption, indicating the likelihood of the tree objects relative to the low-level segments obtained from the CHM image. Certain geometric features are extracted from the underlying segment of each object, and energy functions are proposed to measure how well those features support the object as a plausible tree.

We incorporate the following two energy functions to reflect the assumption: symmetric function $U_d^s(x)$ and area ratio function $U_d^a(x)$. The data term is a weighted sum of the two energy functions, subject to a hard constraint on the object radii, according to the following equation:

$$U_d\mathbf{x} = \begin{cases} \sum_{x \in \mathbf{x}} (w_1 U_d^s(x) + (1 - w_1)U_d^a(x)) & \text{if } r(x) \in [r_m, r_M] \\ +\infty & \text{otherwise} \end{cases} \quad (6)$$

where w_1 is the weight regulating the relative importance of the symmetric and area ratio functions in the data term.

(i) Symmetric function $U_d^s(x)$

A symmetric function is defined as a measure of how well a treetop is located in the central part of the crown and the degree to which the tree crow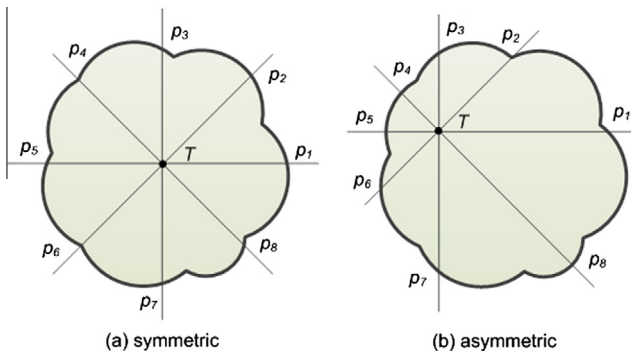n is of a symmetric circular shape. For a given tree object x with corresponding segment s_x, the radii from the treetop point T to the edge of the segment in 8 directions with constant angular intervals $\overline{TP_i}(i = 1, \ldots, 8)$ are first extracted (see Fig. 5). The average and standard deviation of the 8 radii are noted as $r(x)$ and $\Delta r(x)$. The asymmetric ratio $R_{sym}(x) \in [0, 1]$ of object x is calculated as the coefficient of variance of the radii according to the following equation:

$$R_{sym}(x) = \frac{\Delta r(x)}{r(x)} \quad (7)$$

A sigmoid function is then used to define the symmetric function to penalize asymmetric tree crowns given by Eq. (8):

$$U_d^s(x) = \frac{1}{1 + \exp -\left(\frac{R_{sym}(x) - \mu_s}{\lambda_s}\right)} - 1 \quad (8)$$

where μ_s and λ_s are parameters set to control the position and slope of the sigmoid function, respectively. The larger the asymmetric ratio $R_{sym}(x) \in [0, 1]$, the higher the symmetric function score $U_d^s(x) \in [-1, 0]$, which indicates that the treetop is more likely to be a false treetop.

(ii) Area ratio function $U_d^a(x)$

Another area ratio term $U_d^a(x)$ is included to re-enforce the assessment of the geometric features of the objects in the configuration.

Likewise, an area ratio $R_{area} \in [0, 1]$ is first calculated. The ratio is computed as the proportion of the intersection of object x and the underlying segments s_x to the entire area of the segments $A(s_x)$ by Eq. (9). As the area ratio increases, the degree of the geometric feature of the object increases, in accordance with the hypothesis (see Fig. 6).
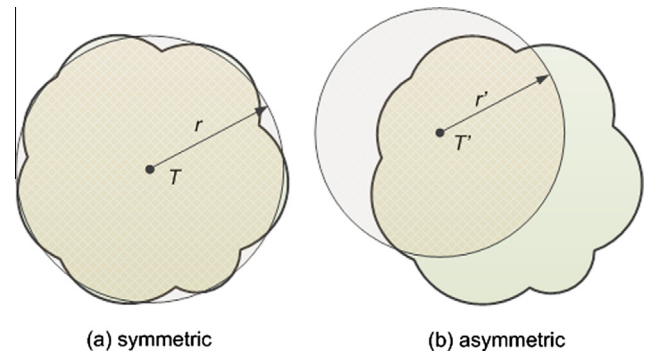

Fig. 5. Asymmetric ratio calculation for (a) symmetric and (b) asymmetric tree crowns.

Fig. 6. Area ratio calculation for tree objects with (a) symmetric and (b) asymmetric tree crowns.

$$R_{area}(x) = \frac{A(x \cap s_x)}{A(s_x)} \tag{9}$$

Based on the area ratio of the object, the area ratio function is defined according to the following equation:

$$U_d^a(x) = \frac{1}{1 + \exp - \left(\frac{R_{area}(x) - \mu_a}{-\lambda_a} \right)} - 1 \tag{10}$$

where μ_a and λ_a are used to control the position and slope of the sigmoid function, respectively.

3.4.2. Prior term

The prior term introduces a *priori* knowledge concerning the layout of the objects. In most mature coniferous forest stands, tree crowns will not overlap too severely. However, overlap between objects should not be totally prohibited. A repulsive term is then defined as a soft penalizing function to penalize severe overlaps in the configuration.

(i) Overlap function $U_p^o(x)$

To define the overlap function, we first introduce a symmetric neighborhood relationship between objects. We say two objects $x_i = (t_i, r_i)$ and $x_j = (t_j, r_j)$ are overlapping if the distance between them is smaller than the sum of their radii, noted as $d(t_i, t_j) < r_i + r_j$, and we write $x_i \sim x_j$. Then, an overlap ratio $R_{overlap} \in [0, 1]$ is calculated as the ratio of the overlap area between the two objects normalized by the area of the smaller object, according to the following equation (see Fig. 7):

$$R_{overlap}(x_i, x_j) = \frac{A(x_i \cap x_j)}{\min(A(x_i), A(x_j))} \tag{11}$$

The overlap score $O(x_i, x_j)$ on $x_i \sim x_j$ is then given according to the following equation:

$$O(x_i, x_j) = \frac{1}{1 + \exp - \left(\frac{R_{overlap}(x_i, x_j) - \mu_o}{\lambda_o} \right)} \tag{12}$$

where μ_o and λ_o are set to control the position and slope of the sigmoid function, respectively.

The overlap function of configuration X can be expressed according to the following equation:

$$U_p^o(\mathbf{x}) = \sum_{x_i \sim x_j} O(x_i, x_j), \forall x_i, x_j \in \mathbf{x}, i \neq j \tag{13}$$

Compared with a classical marked point process, limiting the search space to configurations generated from a subset of a finite set of seed points T (the pre-extracted local maxima) prevents multiple detection problems. The global energy does not have to be designed to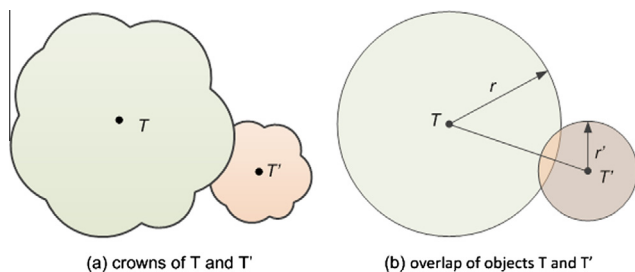 prevent the selection of multiple instances of the same tree because duplicated trees are not part of the search space. Thus, the prior term contains only the overlap function and is written according to the following equation:

$$U_p(\mathbf{x}) = U_p^o(\mathbf{x}) \tag{14}$$

3.5. Parameter estimation

Parameters in the model can be distinguished into the following three categories: physical parameters, weights and thresholds. The physical parameters r_m and r_M are size constraints specifying the range of the tree crown radius in the forest plots. These parameters are set as 1.0 m and 6.0 m, respectively, according to the range of tree sizes in the test sites.

The weights α and w_1 are assigned to tune the relative importance that we want to grant to different energy terms or functions in the combination (see Eqs. (5) and (6)). Both α and w_1 are set to 0.5 because we place equal importance on those functions in all of our experiments.

To reduce the hand-tuned parameters and to avoid a "trial-and-error" test for parameter setting in most practices, we propose a parameter estimation method to estimate the threshold pair (μ, λ) in the sigmoid functions (Eqs. (8), (10) and (12)) in the energy terms. In each function, the threshold pair (μ, λ) controls the tolerance and slope of the sigmoid function, respectively, which plays a significant role in the model. For example, if we set a smaller μ_s value in the symmetric function (Eq. (8)), trees with asymmetric crowns will be penalized more effectively. For a sigmoid function, a smaller value of λ results in a steeper slope, and the associated energy function has an increased discriminative behavior of a step function (see Fig. 8).

We address two issues in the parameter estimation of the energy minimization model. First, the energy terms are designed to penalize false tree objects or implausible configurations with respect to the data term and the prior term. False tree objects or implausible configurations between the objects should receive high energy scores. The parameter estimation is performed by fitting the sigmoid functions to the posterior probability of the features derived from false tree objects or implausible configurations based on the logistic regression model. Second, collection of a large sample size is required to model the posterior probability of those aforementioned features through the Bayesian theorem. In this study, we propose a Monte Carlo-based method, which enables generation of a sufficient number of samples and leads to the estimation of the parameters in the logistic functions.

For example, we will examine the symmetric function $U_d^s(\mathbf{x})$. Let us denote the feature, the asymmetric ratio in this case, extracted from a tree object x_i as d. A random variable $Y = \{0,1\}$ takes the value of 1 if x_i is a true tree object or 0 otherwise. Given an observation d, the probability that the random variable is derived from a false tree object can be given by the posterior probability, according to the following equation:

$$P(Y = 0|d) = \frac{p(d|Y = 0)p(Y = 0)}{p(d)} \tag{15}$$

The higher the posterior probability of the object being a false tree, the higher the energy we assign to the object through the energy functions.

According to the Bayesian theorem, the posterior probability can be rewritten as the following:

$$P(Y = 0|d) = \frac{1}{1 + L_i^o P_i^o} \tag{16}$$

where L_i^o is the likelihood ratio, and P_i^o is the prior ratio, according to the following equations:
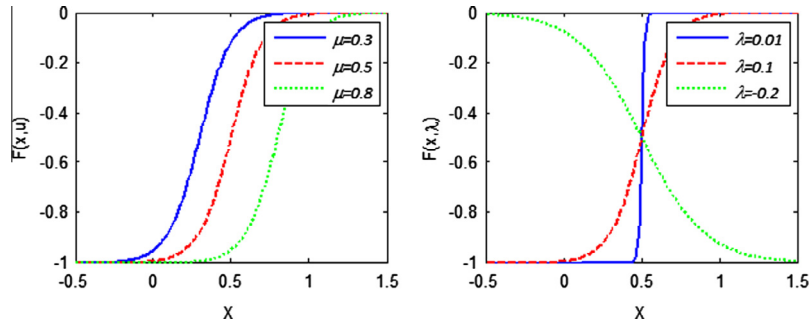

(a) crowns of T and T'   (b) overlap of objects T and T'

Fig. 7. Overlap ratio calculation of overlapping tree crowns.

Fig. 8. Plots of the sigmoid function $F(x) = 1/(1 + \exp = (x - \mu)/\lambda) - 1$ with respect to different values of μ and λ. In the left plot, λ is set to 0.2 for all three curves. In the right plot, μ is set to 0.5 for all three curves.

$$L_i^o = \frac{p(d|Y = 1)}{p(d|Y = 0)} \tag{17}$$

$$P_i^o = \frac{p(Y = 1)}{p(Y = 0)} \tag{18}$$

The likelihood ratio L_i^o can be calculated by modeling the likelihood distributions of features derived from true and false tree objects. A Monte Carlo sampling is utilized to estimate the likelihood distributions. We generate a configurations $\mathbf{x}(T_i)$ from a random subset of local maxima $T_i \subset T$, and $\mathbf{x}(T_i)$ is then compared with the reference configuration $\mathbf{x}(T^o)$. Each tree object $x_j^{T_i}, j = 1, \ldots, n(T_i)$ in configuration $\mathbf{x}(T_i)$ is then labeled as *true* or *false*. We repeat this process for n ($n = 50$ in our experiments) time, to collect enough samples for features of the *true* and *false* tree objects.

The Monte Carlo-based method produces a pool of samples sufficient to model the likelihood distributions of different features. The maximum likelihood method is applied to model the likelihood distributions of the asymmetric ratio, area ratio, and overlap ratio for true and false trees. In practice, we set the prior ratio P_i^o to 2, which is empirically based on the general detection accuracy achieved by LM-based approaches. The modeled distributions and fitted functions are shown in Fig. 9.

3.6. Model optimization

In model optimization, we aim to find the configuration of objects that minimizes the global energy $U(\mathbf{x})$ in the configuration space Ω_T that we have proposed. This discrete configuration space can be effectively explored using a Markov Chain Monte Carlo sampler coupled with simulated annealing.

An MCMC sampler consists in simulating a discrete Markov chain $(X_t), t \in \mathbb{N}$ on the configuration space Ω_T, which converges towards an invariant measure specified by the energy $U(\mathbf{x})$. The sampler performs transitions for one state of the chain to another by proposing a local change of the current configuration.

In our application, a configuration of trees $\mathbf{x}(T^k)$ can be solely determined by a subset of local maxima $T^k \subset T$ given the CHM image. Once treetops are set as the local maxima T^k, the tree sizes are decided and directly derived from the corresponding marker-controlled watershed segments. Therefore, finding the optimal configuration of trees $\mathbf{x}(T^*)$ is equivalent to determining the optimal set of local maxima $T^* \subset T$. The transition of the chain can be managed by a birth-and-death process in which a local maxima is added to or removed from the current set of local maxima T^k to generate a new configuration $\mathbf{x}(T^{k+1})$, from a previous configuration $\mathbf{x}(T^k)$. More specifically,
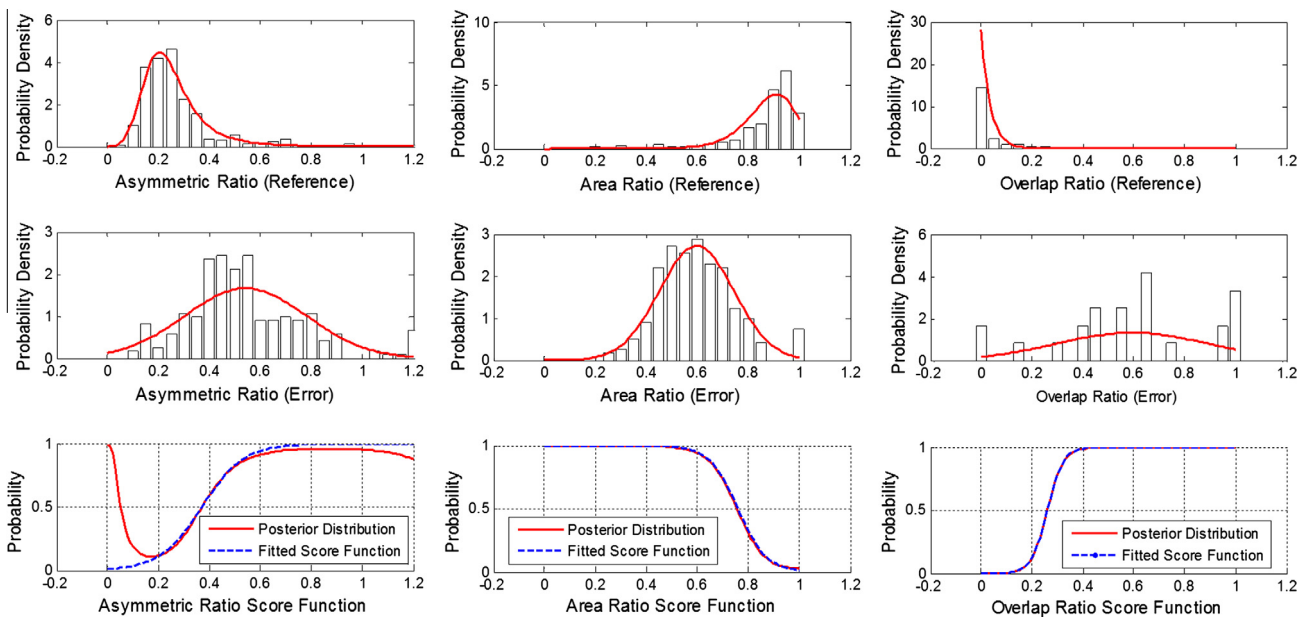
Fig. 9. Likelihood distributions, posterior probability and fitted sigmoid functions for the asymmetric ratio, area ratio and overlap ratio. Row 1: likelihood models of those ratios for the reference group; Row 2: likelihood models of those ratios for the error group; Row 3: posterior probabilities (red lines) for those ratios for the error group and the fitted sigmoid functions (blue dashed lines). (For interpretation of the references to colour in this figure legend, the reader is referred to the web version of this article.)

- In a birth process, a local maxima u is randomly selected from T/T^k and added to the current local maxima set T^k to generate a new configuration $\mathbf{x}(T^{k+1})$, with $T^{k+1} = T^k \cup \{u\}$.
- In a death process, a local maxima v is randomly selected and removed from the current local maxima set T^k to generate a new configuration $\mathbf{x}(T^{k+1})$, with $T^{k+1} = T^k/\{v\}$.

The move between the configurations is symmetric and accepted with the following probability:

$$\min(1, \exp -(U(\mathbf{x}(T^{k+1})) - U(\mathbf{x}))) \tag{19}$$

Otherwise, the previous set of local maxima is kept: $T^{k+1} = T^k$.

A simulated annealing is then embedded in the MCMC to find the optimal configuration with the minimum global energy $U(\mathbf{x})$. To perform the simulated annealing, the Gibbs energy $U(\mathbf{x})$ is replaced with $U_{T_t} = U(\mathbf{x})/T_t$. T_t is the temperature parameter, which tends toward zero as t approaches ∞. A logarithmic decrease ensures the convergence to the global optimum for all of the initial configurations $\mathbf{x}_0$. In practice, a geometric cooling scheme is preferred to accelerate the process and to give an approximate solution close to the optimal one, for example, use $T_t = T_0\alpha^t$ with α close to 1, typically $\alpha = 0.98$.

3.7. Accuracy assessment

To evaluate the performances of the proposed model, the detected trees are compared with the reference data. The comparison results of all of the aggregated trees from the detected trees and the reference data can be classified into the following three categories: the correctly detected trees (correct), trees in the detection results that have no corresponding reference tree (commission) and trees in the reference data not detected (omission). Commission/Omission statistics and the overall detection accuracy are used to quantify the detection results. The calculation of the commission error, omission error and overall accuracy is based on a conventional method of error matrix assessment (Girard, 2003), as shown by Eqs. (20)–(22):

$$\text{Commission error} = \frac{N_{det} - N_{cor}}{N_{det}} \times 100\% \tag{20}$$

$$\text{Commission error} = \frac{N_{ref} - N_{cor}}{N_{ref}} \times 100\% \tag{21}$$

$$\text{Overall quality} = \frac{N_{cor}}{N_{cor} + (N_{det} - N_{cor}) + (N_{ref} - N_{cor})} \times 100\% \tag{22}$$

where N_{cor} is the number of correctly detected trees, N_{det} is the total number of detected trees by the algorithm, and N_{ref} is the number of reference trees.

4. Results

4.1. Parameter estimation results

Table 1 displays the parameters estimated for the energy functions of the proposed model. We then performed experiments with the estimated parameters on real and simulated forest plots to test the robustness of the model.

The parameter μ_s is the threshold in the symmetric function used to penalize tree crowns with high asymmetric ratios. In a forest in which most tree crowns are of regular circular shapes, the value of μ_s can be set relatively smaller to more effectively penalize crowns with asymmetric ratios that exceed this threshold. The threshold μ_a works conversely. Because a larger area ratio indicates a more circular shaped crown, it must be set to a larger value to better penalize tree crowns of a non-circular shape. Parameter μ_o in the overlap function is set to penalize an overlapping situation that exceeds a certain degree, which works similarly to the μ_s parameter. The greater the degree of crown overlap in a forest plot, the larger the μ_o value should be set.

The results shown in Table 1 support this reasoning for parameter setting in which the more the tree crowns in the plot are of symmetric circular shape, the smaller the estimated value of μ_s, whereas the larger the value of μ_a. This reasoning is more explicitly evidenced by the simulated forest plots in which the shape irregularity of the tree crowns increases with the increasing degree of canopy overlap from separated to overlapping, which in turn causes an increase in the value of μ_s from 0.32 to 0.45 and the value of μ_o from 0.08 to 0.40, whereas the value of μ_a decreases correspondingly from 0.82 to 0.72. This result also confirms the rationality of our proposed method for parameter estimation. We also notice that the smaller the overlap degree of a plot, the smaller the estimated λ in the sigmoid function, which indicates a better "threshold" behavior of the associated energy function. This relationship is well in line with the assumption that the simpler the plot situation, the easier the *true* tree crowns and the *false* tree crowns can be distinguished.

From the estimation results of the real and simulated forest plots, we also conclude that the degrees of crown overlap of the real forest plots are between the touch and overlap situations in the simulated forest plots. This condition can be observed from the ranges of the estimated values of μ_s and μ_o of the real forest plots, which are between the parameters estimated for the touch and overlap simulated forest plots.

4.2. Detection results of real forest plots

We first applied the proposed model with the estimated parameters to the ALS data of the three real forest plots. The detection results of local maxima filtering with a variable window size (also referred to as LM) and the proposed model are illustrated in Fig. 10,

Table 1
Parameter estimation results of the proposed model for all of the forest plots.

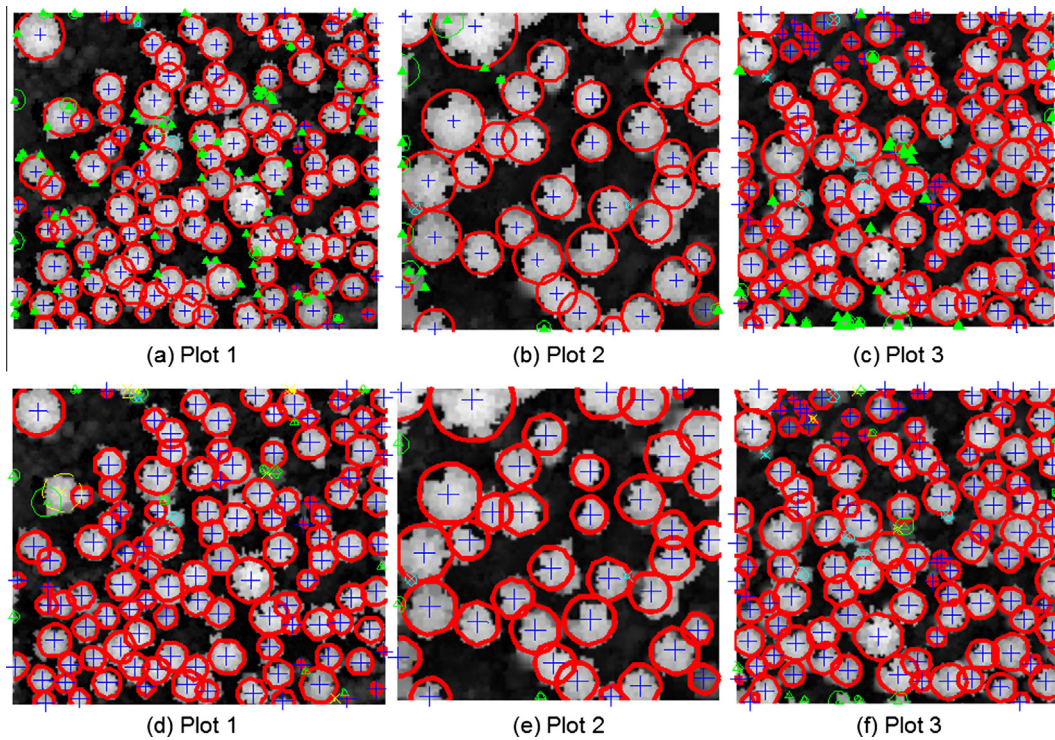|		Parameter estimation					
		Real forest plots			Simulated forest plots		
		Plot 1	Plot 2	Plot3	Separate	Touch	Overlap
Symmetric function	μ_s	0.43	0.39	0.45	0.32	0.37	0.45
	λ_s	0.10	0.11	0.13	0.06	0.08	0.15
Area ratio function	μ_a	0.69	0.68	0.67	0.82	0.76	0.72
	λ_a	−0.07	−0.07	−0.11	−0.03	−0.06	−0.14
Overlap function	μ_o	0.28	0.32	0.38	0.08	0.26	0.40
	λ_o	0.04	0.05	0.05	0.01	0.03	0.05

Fig. 10. Detection results of the proposed model with estimated parameters compared with traditional local maxima filtering on real coniferous forest plots. (a)–(c) Show the local maxima filtering results; (d)–(f) show the detection result of the proposed model using the corresponding local maxima filtering detection as the initial configuration (the green circles with triangles in the center represent the commission errors; the cyan dot line circles represent the omission errors resulting from the LM; the yellow circles represent the omission errors produced by the proposed model). (For interpretation of the references to colour in this figure legend, the reader is referred to the web version of this article.)

which shows a good visual assessment of the performances of the two methods.

The LM results are displayed in the first row (Fig. 10(a)–(c)). In these images, the red circles with blue crosses in the center represent the corrected detected tree crowns, whereas the green and cyan circles represent the commission and omission errors, respectively. Fig. 10 clearly shows that the LM method is prone to produce commission errors in those coniferous forest plots. This problem is particularly noted in plot 1 and plot 3 in which numerous false treetops occur on the edge of tree crowns because of the branching structure of the pine tree species growing in those plots. Plot 2 is a forest with relatively sparser trees, and commission errors primarily occur near the plot boundaries caused by incomplete crown segments and a lack of reference data.

The corresponding images in the second row (Fig. 10(d)–(f)) show the detection results using the proposed model. As can be easily interpreted, most green circles were successfully removed, indicating that the proposed model could effectively reduce the commission errors. We noticed that a small number of yellow dot line circles appear, which indicate trees over-pruned by the proposed model. From the three images, we can observe that the omission errors produced by the proposed model are primarily trees with small crowns and are severely overlapped by their neighboring larger trees. We also noticed that many commission errors occur at the edge of the plots where crowns are shown incomplete or the reference data are missing.

Table 2 depicts the detailed quantitative assessment of the detection results of the LM and the proposed model. There is an obvious improvement in the results of the proposed model over the LM method on which it is based. The commission errors of the three forest plots significantly decreased, with the largest extend in plot 1, decreasing from 36.2% to 10.3%, whereas the omission errors before and after the application of the proposed model remain at similar levels. On average, the overall detection accuracy increased by approximately 15%, comparing results of the proposed model with those of the LM method.

4.3. Detection results of simulated forest plots

The proposed model with the estimated parameters applied to the simulated forest plots exhibited similar detection results to those of the real forest plots. The proposed model significantly reduced the commission errors resulting from the LM method in the three simulated forest plots. Fig. 11 shows a clear contrast in the detection results of the LM and the proposed model.

Similarly, by comparing the corresponding images in Fig. 11(a)–(c) and Fig. 11(d)–(f), it can be observed that nearly all of the green circles (commission errors) in the LM detection results were removed by the proposed model in the three simulated forest plots. Meanwhile, there is only a negligible increase in the number of yellow dot line circles (omission errors). On average, the proposed model increases the overall detection accuracy by approximately 10% compared with the LM method in all of the cases.

Table 3 gives the exact detection results of the LM method and the proposed model on the three simulated plots. It is interesting to examine the influence of the crown overlap degree on the single tree detection results of the LM method. The overall detection accuracy decreases by approximately 10% across the three simulated forest plots with an increasing degree of crown overlap from separated to overlapping. This result is primarily because of the increase in the number of omission errors with the increase in the crown overlap. Trees growing by taller trees are more likely to be missed in the LM detection when crowns are more overlapped. However, the commission errors are less affected by the degree of crown overlap, which remains at a similar level for the three forest plots.

Table 2
Detection results of the proposed model with estimated parameters compared with local maxima filtering (LM) on the real coniferous forest plots.

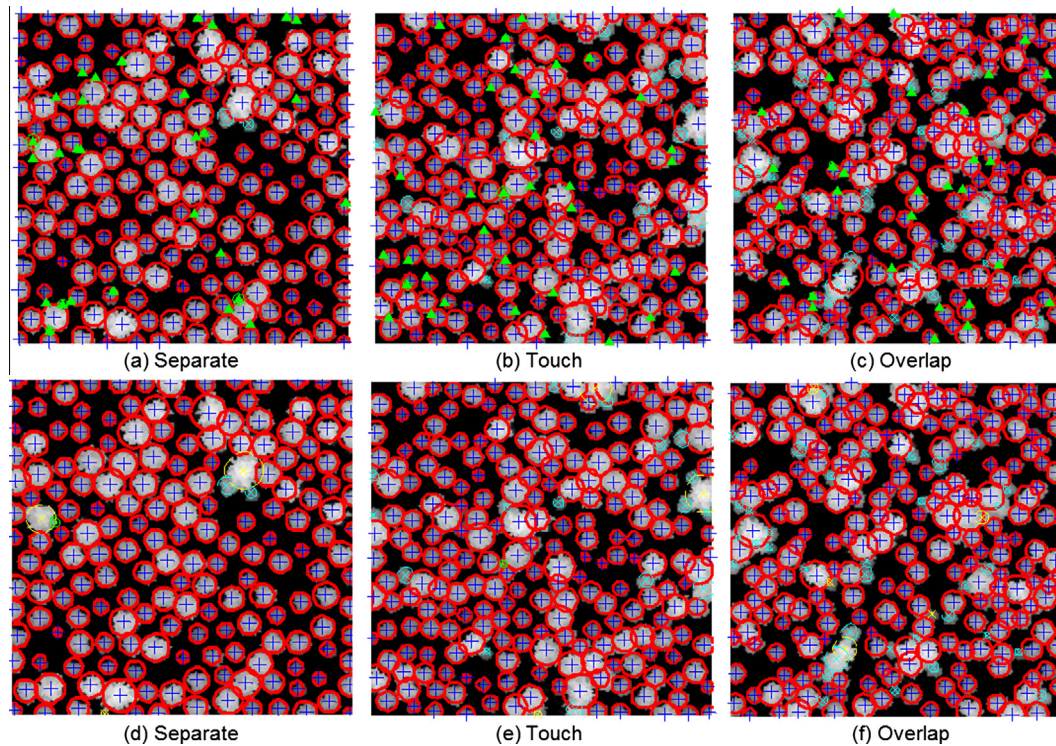| Detected trees		Correct		Commission		Omission		Overall accuracy (%)
		No.	%	No.	%	No.	%	
Plot 1 – 120 trees								
LM	185	118	63.8	67	36.2	2	1.7	63.1
Proposed model	126	113	89.7	13	10.3	7	5.8	85.0
Plot 2 – 40 trees								
LM	51	38	74.5	13	25.5	2	5.0	71.7
Proposed model	41	38	92.7	3	7.3	2	5.0	88.4
Plot 3 – 122 trees								
LM	141	115	81.6	26	18.4	7	5.7	77.7
Proposed model	123	112	91.1	11	8.9	10	8.2	84.2

Fig. 11. Detection results of the proposed model with estimated parameters compared with local maxima filtering on simulated forests. (a)–(c) Show the local maxima filtering detection on the three simulated forest plots; (d)–(f) show the proposed model detection results using the corresponding local maxima filtering detection as the initial configuration (the green circles with triangles in the center represent the commission errors; the cyan dot line circles represent the omission errors resulting from the LM; the yellow circles represent the omission errors produced by the proposed model). (For interpretation of the references to colour in this figure legend, the reader is referred to the web version of this article.)

Table 3
Detection results of the proposed model with estimated parameters compared with local maxima filtering (LM) on the simulated forest plots.

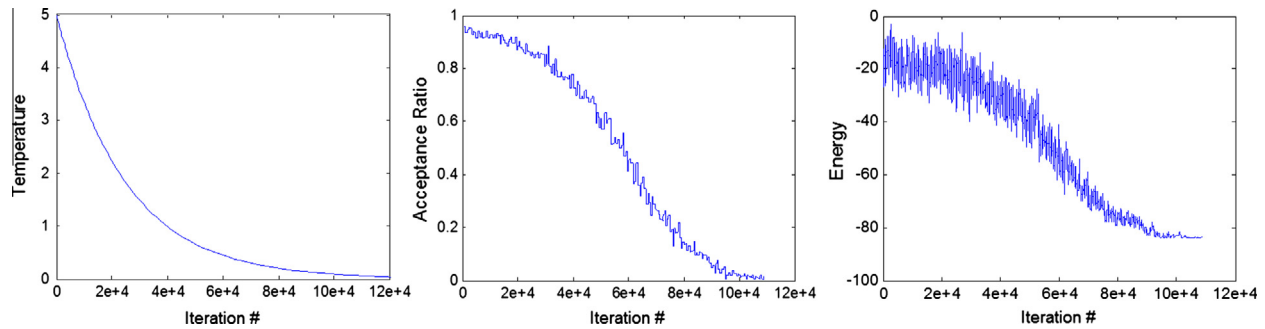| Detected trees		Correct		Commission		Omission		Overall accuracy (%)
		No.	%	No.	%	No.	%	
Separate plot – 186 trees								
LM	213	184	86.4	29	13.6	2	1.1	85.6
Proposed model	182	181	99.5	1	0.5	5	2.7	96.8
Touching plot – 234 trees								
LM	252	218	86.5	34	13.5	16	6.8	81.3
Proposed model	216	215	99.5	1	0.5	19	8.1	91.5
Overlapping plot – 261 trees								
LM	256	226	88.3	30	11.7	35	13.4	77.6
Proposed model	221	221	100.0	0	0.0	40	15.3	84.7

Fig. 12. Statistics associated with the optimization process of the simulated forest plot with touching crowns: (a) temperature; (b) acceptance rate; and (c) global energy.

4.4. Optimization process

Fig. 12 presents the statistics associated with the optimization process, using a simulated forest plot with a touching crown as an example. The plots are at the same abscissa scale to simplify the observation of the optimization process. The iteration index is consistently represented on this axis. In all of the experiments, the temperature decrease coefficient α is set to 0.98, and the temperature is updated every 500 iterations. For a plot with approximately 200 trees, it takes approximately $1.2e + 5$ iterations for the energy to converge, which is significantly fewer than the total number of configurations ($2^{200} \approx 1.6e + 60$) in the entire configuration space. The program takes approximately 3 h to run in Matlab on a processor with a 2.83 GHz frequency.

The first plot (Fig. 12(a)) shows the evolution of the temperature in accordance with a geometric cooling scheme, as described in Section 3.6. Fig. 12(b) represents the acceptance rate associated with the "birth-and-death" kernel. The move acceptance rates are high at the beginning of the process and tend to progressively decrease and stabilize to 0. Finally, Fig. 12(c) plots the global energy. Variations are the highest during the first iterations, and the energy slowly decreases. The decrease becomes faster as the iterations progress and tends to converge slowly to its minimum.

5. Discussion

In this study, we present a hybrid framework to improve the performance of single tree detection from ALS data by taking advantage of low-level image processing techniques and a high-level probabilistic model. The proposed model is applied on the ALS data of real and simulated coniferous forest plots. The results show the feasibility of our approach, and the detection quality is superior to that obtained by the local maxima filtering based method.

The proposed method has been proven to be effective in reduce the commission errors that are introduced by LM in all coniferous forest plots. The LM approach requires a *priori* knowledge of the relationship between the tree height and the crown size, and the detection accuracy can be significantly influenced by the specification of the relationship. In many cases, this relationship is either hard to obtain or different from study to study because it depends on certain factors, such as tree species, tree age, tree density, crown overlapping, and species composition of the forest plot. Moreover, Falkowski et al. (2006) noted that the relationship between the tree height and the crown size can be weak under certain forest conditions, which is coherent with our case. In this case, when a relationship is designated between the tree height and the crown size, the parameters set for the LM are simply a trade-off between commission and omission errors. We suggested a relative small window size for the LM to over-extract initial 'treetops' at the first stage, and the embedded

probabilistic model showed its powerfulness in excluding the false treetops from the final configuration through stochastic inference by considering the spatial layouts and geometric characteristics of the trees in the forest plots.

Simulation of forest plots and ALS data provide a valuable tool to examine the performance of tree detection methods under the influence of stem densities and degrees of crown overlap. The detection results evidence the higher the stem density, the more likely the tree crowns are overlapped in the plot, causing smaller trees growing nearby larger trees not easily be detected. The results obtained are coherent with those reported in other studies that denser plots give less accuracy results than sparse plots. The simulated data also provides a fully controlled environment to observe the behavior of the estimated parameters in the designed energy functions with respect to the factor of crown overlap. The increase in crown overlap results in more asymmetric crowns in CHM, which are noted by the estimated parameters and further validate the rationality of the parameter estimation method we proposed. The simulation in our study is intended to test our proposed model under certain key forest variables, i.e., the tree density and crown overlap in our case. Additional sophisticated simulations of forest structure and ALS returns can be found in Morsdorf et al. (2009) and Disney et al. (2010).

The detection of single trees from remote sensing data using marked point processes was first performed by Andersen et al. (2002) in an attempt to directly detect trees of a coniferous plot from ALS point clouds using the marked point process in a Bayesian framework. The results have indicated that the algorithm is generally successful in identifying structures associated with individual tree crowns within the forest plot but appears to be sensitive to complex point cloud data. Perrin et al. (2005, 2006) has employed marked point processes to detect tree crowns from CIR aerial imageries of plantations, which leads to a continuous search space for the tree objects, in contrast to the proposed method.

The stochastic model we proposed is the first to integrate low-level image processing techniques and a high-level probabilistic model into a hybrid framework for single tree detection. The model assembles marked point processes in terms of object modeling and energy formulation. However, in the model, the parameters of the tree objects are directly derived from low-level representations of LiDAR images produced by traditional image processing techniques rather than random sampling in classical marked point processes. Thus, the model generates a constrained discrete configuration space, in which we sample for the global optimum that contains the final set of detected trees. In this manner, the computation cost is significantly reduced, and the optimization process can be significantly accelerated.

The design of proper energy terms is an important issue we attempt to address due to the different types of data we used and the specific manner in which we constructed a configuration. The models used to detect tree crowns in aerial imageries (Perrin

et al., 2005, 2006) make use of the distinctive pixel values between the illuminated area near the center of the tree crowns and that of the backgrounds or valleys between the crowns. The contrast between the tree crowns and the background, or treetop areas and valleys between them, can be exaggerated by shadows and stretched spectral or radiometric characteristics in the optical images. However, the elevation differences between those parts in the CHM images are much milder and complex to model than the contrasts in optical imageries. This fact is also the reason we chose a Gibbs energy to measure the morphological characteristics of the tree objects in a configuration, other than a Bayesian framework to model height distributions, considering the complexity required to design a height model valid for all of the trees of various heights and crown forms in the forest area.

Parameter estimation is another challenging task in most stochastic models. In this study, we proposed a Monte Carlo-based method to estimate certain key parameters in our model. The Monte Carlo simulation was used to generate random configurations and to create a sufficient number of samples of true and false tree crowns, which enabled the modeling of feature distributions of true and false tree crowns to estimate thresholds in the energy terms. The experimental results on all of the datasets, especially the simulated ones, suggested that the parameter estimation method works reasonably well.

The proposed method has certain inherited drawbacks detecting trees from the rasterized canopy height model, which is incapable of finding suppressed trees under dominant crowns (Hyyppä et al., 2012). The method is designed to detect trees in the dominant layers in the coniferous forest plots of interest. Exploiting 3D information from the ALS point cloud to detect small trees in the lower forest layer is a possible direction to overcome this disadvantage (Ferraz et al., 2012; Reitberger et al., 2009). Another limitation of the method is that it is unable to recover the omission error produced by local maxima filtering on which it is based. Because tree positions are constrained within the pre-extracted local maxima, the model experienced a reduced ability in the classical marked point process to sample the configuration space more thoroughly. However, experimental results on real and simulated forest plots still suggest that the proposed model is a good compromise regarding complexity, efficiency and accuracy.

6. Conclusions and future studies

We propose a hybrid framework to detect single trees from ALS data by combining the low-level image processing techniques of LM and MCWS with a high-level probabilistic model. More specifically, in this model, tree crowns in an ALS recovered CHM are modeled as objects and are considered as a configuration of circles. The probabilistic model enables the consideration of the geometric characteristics and the pair-wise interactions of objects in the configuration. The LM and MCWS are employed to produce a low-level representation of the image, which provides a constrained configuration space for the probabilistic model to sample for the optimal configuration. We also propose a Monte Carlo-based method to estimate important parameters in the proposed model. The model is proven effective when applied to real and simulated coniferous forest plots. The results show that the proposed model has a distinct improvement in the detection quality over the traditional local maxima filtering based approach by approximately 10% on all of the datasets.

Future studies should involve a further examination of the optimization methods. An important benefit we gained from our proposed model is that the configuration space is significantly reduced by incorporating features extracted from the CHM image through low-level image processing techniques. However, there remains a significant requirement to accelerate the optimization process. A prior-guided MCMC or a steepest gradient descent algorithm are possibilities we will examine to accelerate the search for the optimal configuration within the discrete configuration space. Second, post-processing will be introduced to recover omission errors from the detection results. Although the proposed model was proven effective in reducing commission errors, the tree positions are constrained in the predetermined set of the local maxima extracted by local maxima filtering. It is possible to recover a portion of the omitted trees from the detected results because those missed crowns will result in more geometrically irregular segments. Finally, automated segmentation of forest stands into homogenous areas with similar forest conditions can be introduced to help train parameters of the proposed model of representative regions and make the model applicable to larger areas. We will also further test the proposed model on more datasets of different forest types and conditions.

References

Andersen, H.-E., Reutebuch, S.E., Schreuder, G.F., 2002. Bayesian object recognition for the analysis of complex forest scenes in airborne laser scanner data. Int. Arch. Photogrammetry Remote Sens., 35–41.

Bortolot, Z.J., Wynne, R.H., 2005. Estimating forest biomass using small footprint LiDAR data: an individual tree-based approach that incorporates training data. ISPRS J. Photogrammetry Remote Sens. 59, 342–360.

Brandtberg, T., 2007. Classifying individual tree species under leaf-off and leaf-on conditions using airborne lidar. ISPRS J. Photogrammetry Remote Sens. 61, 325–340.

Brandtberg, T., Walter, F., 1998. Automated delineation of individual tree crowns in high spatial resolution aerial images by multiple-scale analysis. Mach. Vis. Appl. 11, 64–73.

Brandtberg, T., Warner, T.A., Landenberger, R.E., McGraw, J.B., 2003. Detection and analysis of individual leaf-off tree crowns in small footprint, high sampling density lidar data from the eastern deciduous forest in North America. Remote Sens. Environ. 85, 290–303.

Breidenbach, J., Næsset, E., Lien, V., Gobakken, T., Solberg, S., 2010. Prediction of species specific forest inventory attributes using a nonparametric semi-individual tree crown approach based on fused airborne laser scanning and multispectral data. Remote Sens. Environ. 114, 911–924.

Chen, Q., Baldocchi, D., Gong, P., Kelly, M., 2006. Isolating individual trees in a savanna woodland using small footprint lidar data. Photogrammetric Eng. Remote Sens. 72, 923–932.

Descombes, X., Pechersky, E., 2006. Tree Crown Extraction Using a Three State Markov Random Field.

Descombes, X., Zerubia, J., 2002. Marked point process in image analysis. IEEE Signal Process. Mag. 19, 77–84.

Disney, M.I., Kalogirou, V., Lewis, P., Prieto-Blanco, A., Hancock, S., Pfeifer, M., 2010. Simulating the impact of discrete-return lidar system and survey characteristics over young conifer and broadleaf forests. Remote Sens. Environ. 114, 1546–1560.

Dubayah, R.O., Drake, J.B., 2000. Lidar remote sensing for forestry applications. J. Forest 98, 44–46.

Erikson, M., 2003. Segmentation of individual tree crowns in colour aerial photographs using region growing supported by fuzzy rules. Can. J. For. Res. 33, 1557–1563.

Falkowski, M.J., Smith, A.M.S., Hudak, A.T., Gessler, P.E., Vierling, L.A., Crookston, N.L., 2006. Automated estimation of individual conifer tree height and crown diameter via two-dimensional spatial wavelet analysis of lidar data. Can. J. Remote Sens. 32, 153–161.

Ferraz, A., Bretar, F., Jacquemoud, S., Gonçalves, G., Pereira, L., Tomé, M., Soares, P., 2012. 3-D mapping of a multi-layered mediterranean forest using ALS data. Remote Sens. Environ. 121, 210–223.

Gebreslasie, M.T., Ahmed, F.B., van Aardt, J.A.N., Blakeway, F., 2011. Individual tree detection based on variable and fixed window size local maxima filtering applied to IKONOS imagery for even-aged eucalyptus plantation forests. Int. J. Remote Sens. 32, 4141–4154.

Girard, M.C., 2003. Processing of Remote Sensing Data. Taylor & Francis, London.

Gleason, C.J., Im, J., 2012. A fusion approach for tree crown delineation from lidar data. Photogrammetric Eng. Remote Sens. 78, 679–692.

Gonzalez, R.C., Woods, R.E., 2008. Digital Image Processing, third ed. Pearson/Prentice Hall, Upper Saddle River, NJ.

Gougeon, F.A., 1995. A crown-following approach to the automatic delineation of individual tree crowns in high spatial resolution aerial images. Can. J. Remote Sens. 21, 274–284.

Hastings, W.K., 1970. Monte Carlo sampling methods using Markov chains and their applications. Biometrika 57, 97–109.

Heinzel, J., Koch, B., 2011. Exploring full-waveform LiDAR parameters for tree species classification. Int. J. Appl. Earth Obs. Geoinf. 13, 152–160.

Heurich, M., 2008. Automatic recognition and measurement of single trees based on data from airborne laser scanning over the richly structured natural forests of the Bavarian Forest National Park. For. Ecol. Manage. 255, 2416–2433.

Hyyppä, J., Inkinen, M., 1999. Detecting and estimating attributes for single trees using laser scanner. Photogrammetric J. Finland 16, 27–42.

Hyyppä, J., Kelle, O., Lehikoinen, M., Inkinen, M., 2001. A segmentation-based method to retrieve stem volume estimates from 3-D tree height models produced by laser scanners. Geosci. Remote Sens., IEEE Trans. 39, 969–975.

Hyyppä, J., Hyyppä, H., Leckie, D., Gougeon, F., Yu, X., Maltamo, M., 2008. Review of methods of small-footprint airborne laser scanning for extracting forest inventory data in boreal forests. Int. J. Remote Sens. 29, 1339–1366.

Hyyppä, J., Yu, X., Hyyppä, H., Vastaranta, M., Holopainen, M., Kukko, A., Kaartinen, H., Jaakkola, A., Vaaja, M., Koskinen, J., Alho, P., 2012. Advances in forest inventory using airborne laser scanning. Remote Sens. 4, 1190–1207.

Kaartinen, H., Hyyppä, J., Yu, X., Vastaranta, M., Hyyppä, H., Kukko, A., Holopainen, M., Heipke, C., Hirschmugl, M., Morsdorf, F., Næsset, E., Pitkänen, J., Popescu, S., Solberg, S., Wolf, B.M., Wu, J.C., 2012. An international comparison of individual tree detection and extraction using airborne laser scanning. Remote Sens. 4, 950–974.

Korpela, I., Dahlin, B., Schäfer, H., Bruun, E., Haapaniemi, F., Honkasalo, J., Ilvesniemi, S., Kuutti, V., Linkosalmi, M., Mustonen, J., 2007. Single-tree forest inventory using lidar and aerial images for 3D treetop positioning, species recognition, height and crown width estimation. Int. Arch. Photogrammetry Remote Sens. Spatial Inf. Sci., 227–233.

Lacoste, C., Descombes, X., Zerubia, J., 2005. Point processes for unsupervised line network extraction in remote sensing. Pattern Anal. Machine Intell., IEEE Trans. 27, 1568–1579.

Lafarge, F., Descombes, X., Zerubia, J., Pierrot-Deseilligny, M., 2008. Automatic building extraction from DEMs using an object approach and application to the 3D-city modeling. ISPRS J. Photogrammetry Remote Sens. 63, 365–381.

Leckie, D., Gougeon, F., Hill, D., Quinn, R., Armstrong, L., Shreenan, R., 2003. Combined high-density lidar and multispectral imagery for individual tree crown analysis. Can. J. Remote Sens. 29, 633–649.

Maltamo, M., Malinen, J., Packaln, P., Suvanto, A., Kangas, J., 2006. Nonparametric estimation of stem volume using airborne laser scanning, aerial photography, and stand-register data. Can. J. Forest Res. 36, 426–436.

Means, J.E., Acker, S.A., Fitt, B.J., Renslow, M., Emerson, L., Hendrix, C.J., 2000. Predicting forest stand characteristics with airborne scanning lidar. Photogrammetric Eng. Remote Sens. 66, 1367–1371.

Metropolis, N., Rosenbluth, A.W., Rosenbluth, M.N., Teller, A.H., Teller, E., 1953. Equation of state calculations by fast computing machines. J. Chem. Phys. 21, 1087–1092.

Meyer, F., Beucher, S., 1990. Morphological segmentation. J. Vis. Commun. Image Represent. 1, 21–46.

Morsdorf, F., Nichol, C., Malthus, T., Woodhouse, I.H., 2009. Assessing forest structural and physiological information content of multi-spectral LiDAR waveforms by radiative transfer modelling. Remote Sens. Environ. 113, 2152–2163.

Næsset, E., 1997. Determination of mean tree height of forest stands using airborne laser scanner data. ISPRS J. Photogrammetry Remote Sens. 52, 49–56.

Naesset, E., 2002. Predicting forest stand characteristics with airborne scanning laser using a practical two-stage procedure and field data. Remote Sens. Environ. 80, 88–99.

Naesset, E., 2004. Practical large-scale forest stand inventory using a small-footprint airborne scanning laser. Scand. J. Forest Res. 19, 164–179.

Naesset, E., Gobakken, T., Holmgren, J., Hyyppa, H., Hyyppa, J., Maltamo, M., Nilsson, M., Olsson, H., Persson, A., Soderman, U., 2004. Laser scanning of forest resources: the nordic experience. Scand. J. Forest Res. 19, 482–499.

Orka, H.O., Naesset, E., Bollandsas, O.M., 2009. Classifying species of individual trees by intensity and structure features derived from airborne laser scanner data. Remote Sens. Environ. 113, 1163–1174.

Ortner, M., Descombes, X., Zerubia, J., 2008. A marked point process of rectangles and segments for automatic analysis of digital elevation models. Pattern Anal. Machine Intell., IEEE Trans. 30, 105–119.

Perrin, G., Descombes, X., Zerubia, J., 2005. Point processes in forestry: an application to tree crown detection. INRIA.

Perrin, G., Descombes, X., Zerubia, J., 2006. A non-Bayesian model for tree crown extraction using marked point processes.

Pollock, R., 1996. The Automatic Recognition of Individual Trees in Aerial Images of Forests Based on a Synthetic Tree Crown Image Model, Computer Science. University of British Columbia.

Popescu, S.C., Wynne, R.H., Nelson, R.F., 2002. Estimating plot-level tree heights with lidar: local filtering with a canopy-height based variable window size. Comput. Electron. Agr. 37, 71–95.

Pyysalo, U., Hyyppa, H., 2002. Reconstructing tree crowns from laser scanner data for feature extraction. Int. Arch. Photogrammetry Remote Sens. Spatial Inf. Sci. 34, 218–221.

Reitberger, J., Schnörr, C., Krzystek, P., Stilla, U., 2009. 3D segmentation of single trees exploiting full waveform LIDAR data. ISPRS J. Photogrammetry Remote Sens. 64, 561–574.

Solberg, S., Naesset, E., Bollandsas, O.M., 2006. Single tree segmentation using airborne laser scanner data in a structurally heterogeneous spruce forest. Photogrammetric Eng. Remote Sens. 72, 1369–1378.

Sonka, M., Hlavac, V., Boyle, R., 2008. Image Processing, Analysis, and Machine Vision, third ed. Thompson Learning, Toronto.

Suratno, A., Seielstad, C., Queen, L., 2009. Tree species identification in mixed coniferous forest using airborne laser scanning. ISPRS J. Photogrammetry Remote Sens. 64, 683–693.

Tomppo, E., Nilsson, M., Rosengren, M., Aalto, P., Kennedy, P., 2002. Simultaneous use of Landsat-TM and IRS-1C WiFS data in estimating large area tree stem volume and aboveground biomass. Remote Sens. Environ. 82, 156–171.

Tournaire, O., Paparoditis, N., 2009. A geometric stochastic approach based on marked point processes for road mark detection from high resolution aerial images. ISPRS J. Photogrammetry Remote Sens. 64, 621–631.

Tournaire, O., Brédif, M., Boldo, D., Durupt, M., 2010. An efficient stochastic approach for building footprint extraction from digital elevation models. ISPRS J. Photogrammetry Remote Sens. 65, 317–327.

Van Lieshout, M.N.M., 2000. Markov Point Process and their Applications. Imperial College Press, London.

Van Lieshout, M.N.M., 2009. Applications of stochastic geometry in image analysis. In: Kendall, W.S., Molchanov, I. (Eds.), New Perspectives in Stochastic Geometry. Oxford University Press, pp. 427–450.

Vastaranta, M., Holopainen, M., Yu, X., Haapanen, R., Melkas, T., Hyyppä, J., Hyyppä, H., 2011a. Individual tree detection and area-based approach in retrieval of forest inventory characteristics from low-pulse airborne laser scanning data. Photogram. J. Fin. 22, 1–13.

Vastaranta, M., Holopainen, M., Yu, X.W., Hyyppa, J., Makinen, A., Rasinmaki, J., Melkas, T., Kaartinen, H., Hyyppa, H., 2011b. Effects of individual tree detection error sources on forest management planning calculations. Remote Sens. 3, 1614–1626.

Vastaranta, M., Kankare, V., Holopainen, M., Yu, X., Hyyppä, J., Hyyppä, H., 2012. Combination of individual tree detection and area-based approach in imputation of forest variables using airborne laser data. ISPRS J. Photogrammetry Remote Sens. 67, 73–79.

Vauhkonen, J., Ene, L., Gupta, S., Heinzel, J., Holmgren, J., Pitkanen, J., Solberg, S., Wang, Y.S., Weinacker, H., Hauglin, K.M., Lien, V., Packalen, P., Gobakken, T., Koch, B., Naesset, E., Tokola, T., Maltamo, M., 2012. Comparative testing of single-tree detection algorithms under different types of forest. Forestry 85, 27–40.

Wang, L., Gong, P., Biging, G.S., 2004. Individual tree-crown delineation and treetop detection in high-spatial-resolution aerial imagery. Photogrammetric Eng. Remote Sens. 70, 351–358.

White, J., Wulder, M., Vastaranta, M., Coops, N., Pitt, D., Woods, M., 2013. The utility of image-based point clouds for forest inventory: a comparison with airborne laser scanning. Forests 4, 518–536.

Wulder, M., 1998. Optical remote-sensing techniques for the assessment of forest inventory and biophysical parameters. Prog. Phys. Geogr. 22, 449–476.

Wulder, M., Niemann, K.O., Goodenough, D.G., 2000. Local maximum filtering for the extraction of tree locations and basal area from high spatial resolution imagery. Remote Sens. Environ. 73, 103–114.

Xie, Y., Sha, Z., Yu, M., 2008. Remote sensing imagery in vegetation mapping: a review. J. Plant Ecol. 1, 9–23.

Yao, W., Krzystek, P., Heurich, M., 2012. Tree species classification and estimation of stem volume and DBH based on single tree extraction by exploiting airborne full-waveform LiDAR data. Remote Sens. Environ. 123, 368–380.

Yu, X.W., Hyyppa, J., Kaartinen, H., Maltamo, M., 2004. Automatic detection of harvested trees and determination of forest growth using airborne laser scanning. Remote Sens. Environ. 90, 451–462.

Yu, X.W., Hyyppa, J., Holopainen, M., Vastaranta, M., 2010. Comparison of area-based and individual tree-based methods for predicting plot-level forest attributes. Remote Sens. 2, 1481–1495.

Zhang, J., Sohn, G., 2010. A comparison of single tree detection algorithm using simulated and real samples, Silvilaser 2010, the 10th International Conference on LiDAR Applications for Assessing Forest Ecosystems, Freiburg, Germany, pp. 480–488.